Supporting information

Active Site Exploration of Core–Corona Structured Bifunctional Cobalt Ferrite–Containing Nitrogen-Doped Carbon Nanotubes for Rechargeable Zinc–Air Battery Application

Shankar Baskaran, [a] E. A. Anook Nazer [a] and Azhagumuthu Muthukrishnan *,[a]

[a]School of Chemistry, Indian Institute of Science Education and Research Thiruvananthapuram, Maruthamala P.O., Vithura 695551, Kerala, India

Email: muthukrishnan@iisertvm.ac.in

Table of contents

Chemicals

The following chemicals were purchased and used for the synthesis

1. $Fe(NO_3)_3.9H_2O$ (98%), from Merck, India
2. $Co(NO_3)_2.6H_2O$ (98%), from Merck, India
3. $FeSO_4.7H_2O$ (99%), from Merck, India
4. $FeCl_3.6H_2O$ (98%) from Merck, India
5. Methanol (99%), from Merck, India
6. 2-methylimidazole (98%), from Avra synthesis, India
7. $Zn(NO_3)_2.6H_2O$ (98%), from Avra synthesis, India
8. NaOH pellets (97%), from Spectrochem, India.

Synthesis of Fe_3O_4

The mixture of $FeSO_4.7H_2O$ (55 mg) and $FeCl_3.6H_2O$ (100 mg) was dissolved in 20 ml of distilled water and stirred for 30 minutes. Add 10 ml of 3 M NaOH solution with this solution and stir overnight. A black colour precipitate was formed and separated by centrifugation, and washed with water and ethanol. The precipitate was dried in a vacuum oven at 60 ºC for 12 hours. Thus, formed Fe_3O_4 was confirmed using PXRD (Figure S10a).

Synthesis of Co_3O_4

A solution of $Co(NO_3)_2.6H_2O$ (4.3 g) in 15 ml water was prepared, and 15 ml of 3 M NaOH was added. The mixture was heated to 60 ºC for 4 hours under stirring. A black colour precipitate was separated by centrifugation and washed with water and ethanol. It was dried in a vacuum oven at 80 ºC overnight. The product was finely powdered and calcined at 700 ºC for 4 hours to obtain Co_3O_4,[16] confirmed by PXRD (Figure S10b).

Material characterisation

The crystalline nature of N-doped carbon and $CoFe_2O_4$ were studied using X-ray diffraction by Bruker Powder-XRD using Cu Kα source. The morphology of the samples was studied using Nova NANOSEM 450. Further, the transmission electron microscopy (TEM) analysis was performed to study the morphology using FEI Tecnai G2 Spirit Bio-Twin TEM 300 kV. The Raman spectroscopy was used to study the carbon defects by HR800 LabRAM confocal Raman spectrometer. The thermogravimetric analysis was performed using TA instruments

SDT. The surface area and porosity analysis were performed using the Micromeritics 3Flex system at 77 K. The X-ray photoelectron spectroscopy (XPS) measurements were done using Omicron Nanotech instrument with Mg Kα excitation source (1253.6 eV) in a CAE mode with a pass energy of 50 eV.

The number of electrons (n) involved in reducing per oxygen molecule and the percentage of H_2O_2 intermediate were calculated from the disc (I_D) and ring (I_R) currents

$$n = \frac{4I_D}{I_D + \frac{I_R}{N}} \qquad (1)$$

$$\% \, H_2O_2 = \frac{\frac{2I_R}{N}}{I_D + \frac{I_R}{N}} \times 100 \qquad (2)$$

where N is the collection efficiency (0.37) of the ring electrode.

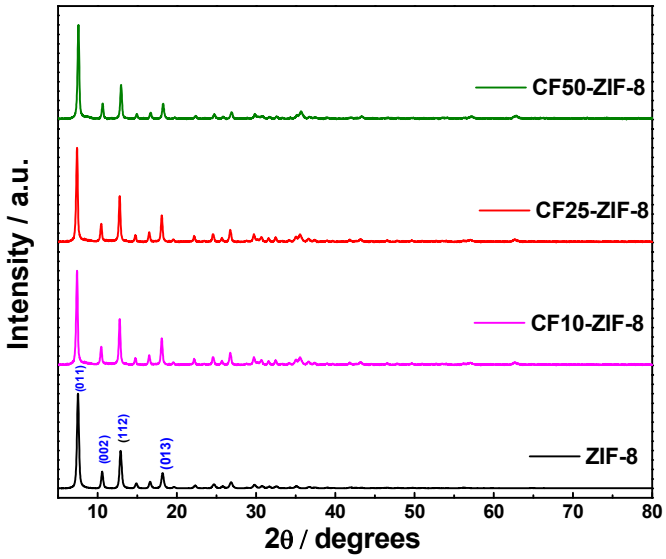

Figure S1. Power XRD patterns of pure ZIF-8 and $CoFe_2O_4$-ZIF-8 composites

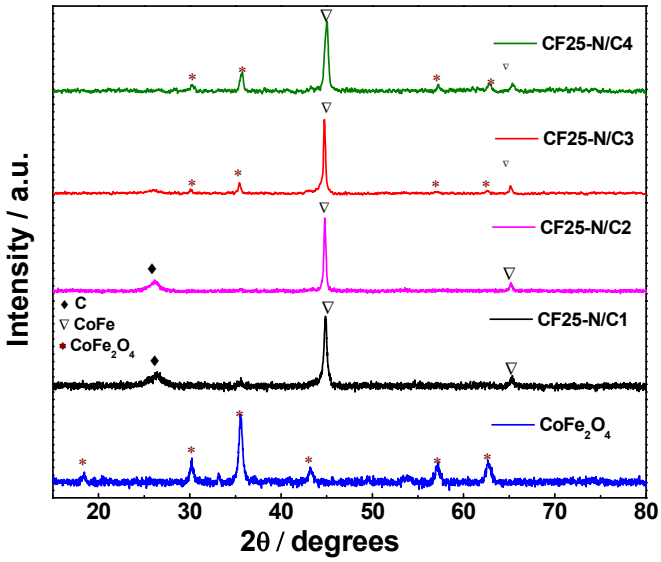

Figure S2. Powder XRD patterns of CF25-ZIF-8 pyrolyzed to 900 ^{0}C of various dwelling time

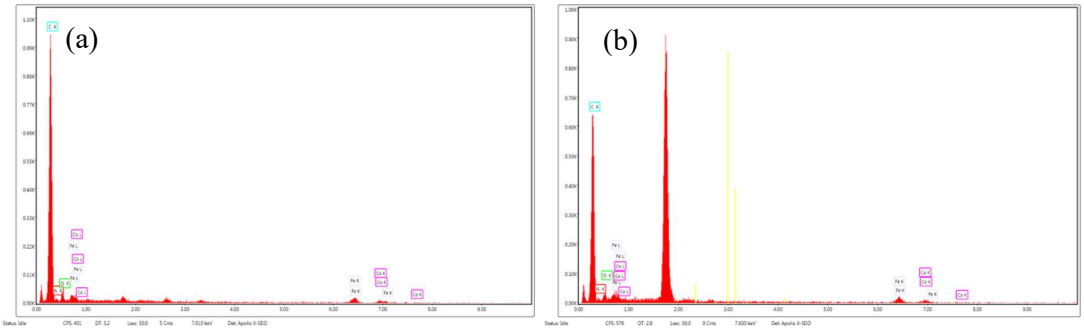

Figure S3. Energy dispersive X-ray spectroscopy of (a) CF10-N/C4 and (b) CF25-N/C4 materials

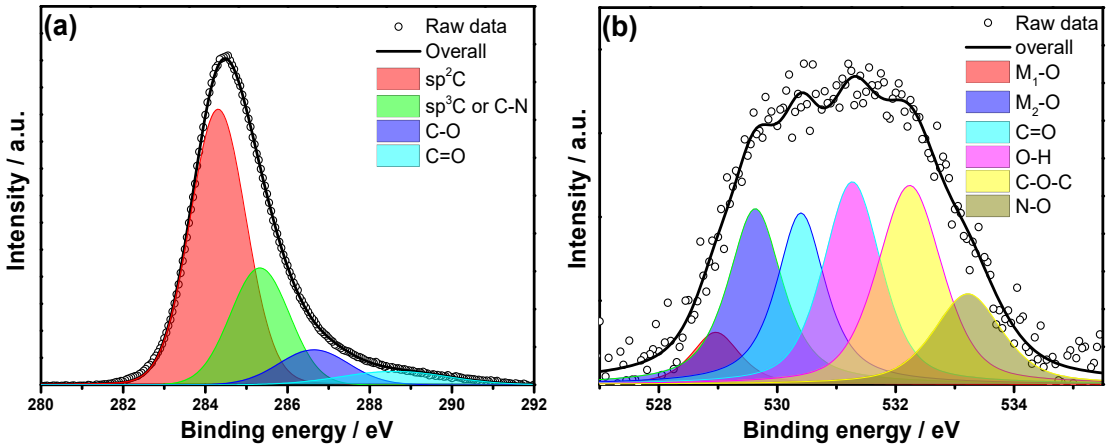

Figure S4. (a) C1s and (b) O-1s XPS of CF10-N/C4 material and their deconvoluted peaks referring to various bonding nature of carbon and oxygen.

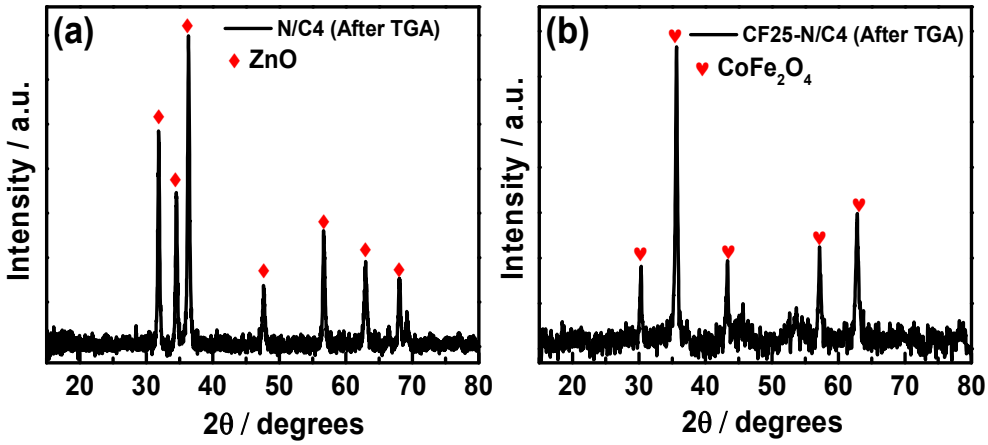

Figure S5. Powder XRD patterns of (a) N/C4 and (b) CF25-N/C4 after the thermogravimetric analysis under the airflow.

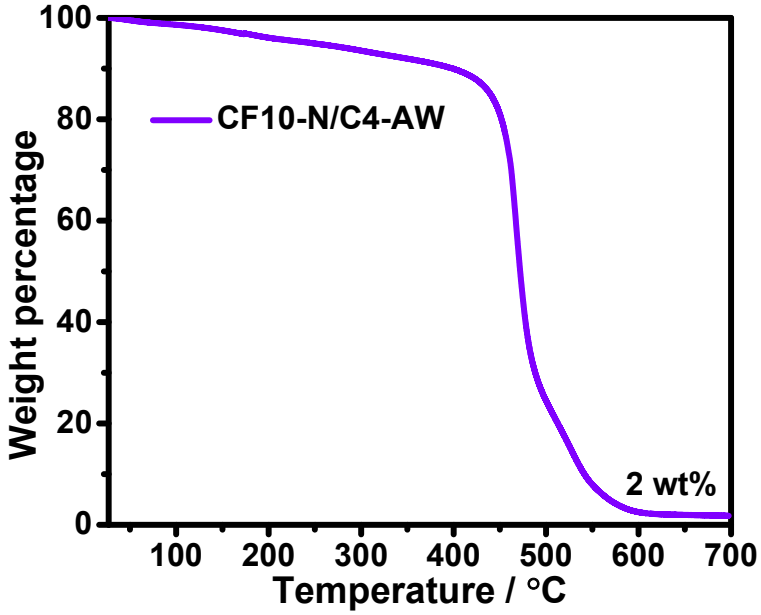

Figure S6. TGA curve of CF10-N/C4-AW composite

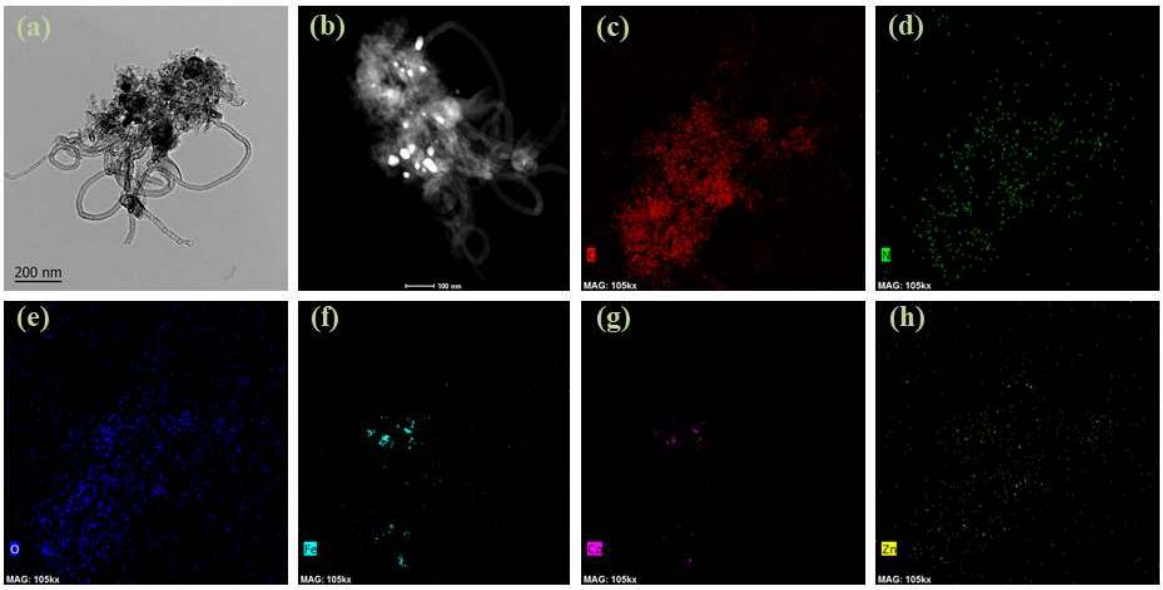

Figure S7. HR-TEM image of (a) CF10-N/C4-AW and (b) HAADF image. The EELS elemental mapping of CF10-N/C4-AW for (c) C, (d) N, (e) O, (f) Fe, (g) Co and (h) Zn.

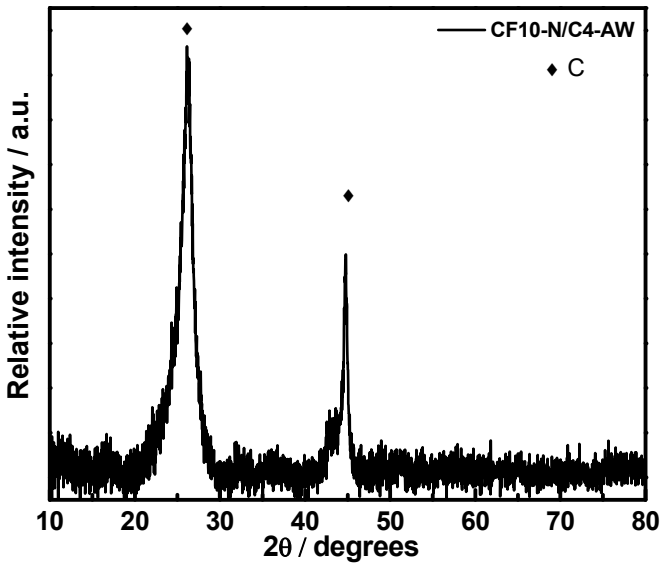

Figure S8. Powder XRD pattern of CF10-N/C4-AW material

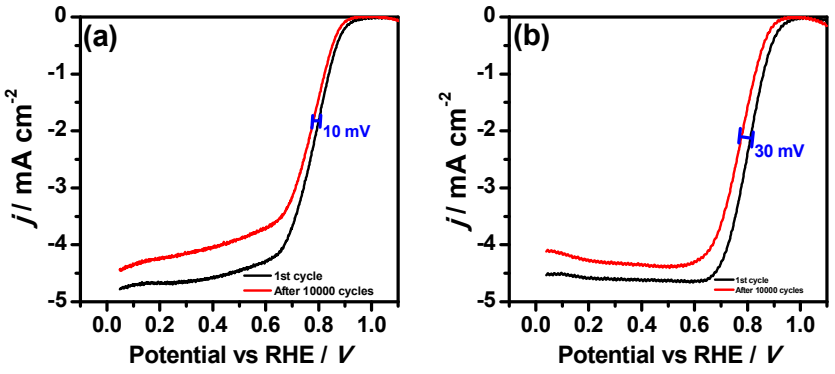

Figure S9. The rotating disk electrode voltammograms of (a) CF10-N/C4 and (b) CF10-N/C4-AW before (black trace) and after (red trace) the stability test (10,000 cycles).

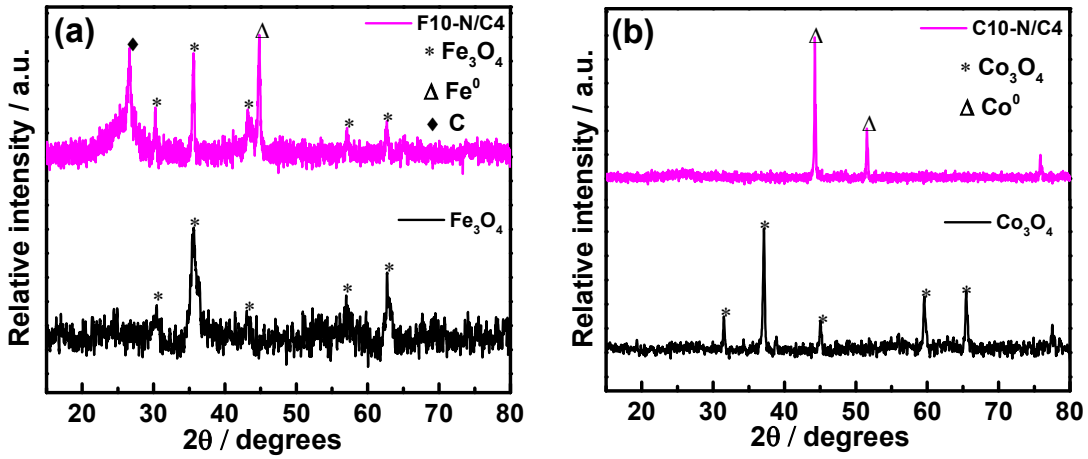

Figure S10. The powder XRD patterns of (a) Fe_3O_4 (black trace) and F10-N/C4 (pink trace). (b) The powder XRD patterns of Co_3O_4 (black trace) and C10-N/C4 (pink trace).

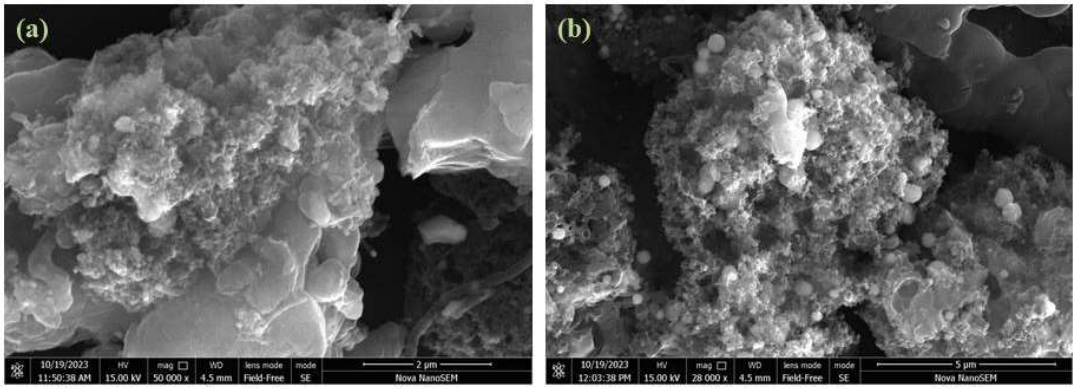

Figure S11. The SEM images of (a) F10-N/C4 and (b) C10-N/C4 materials.

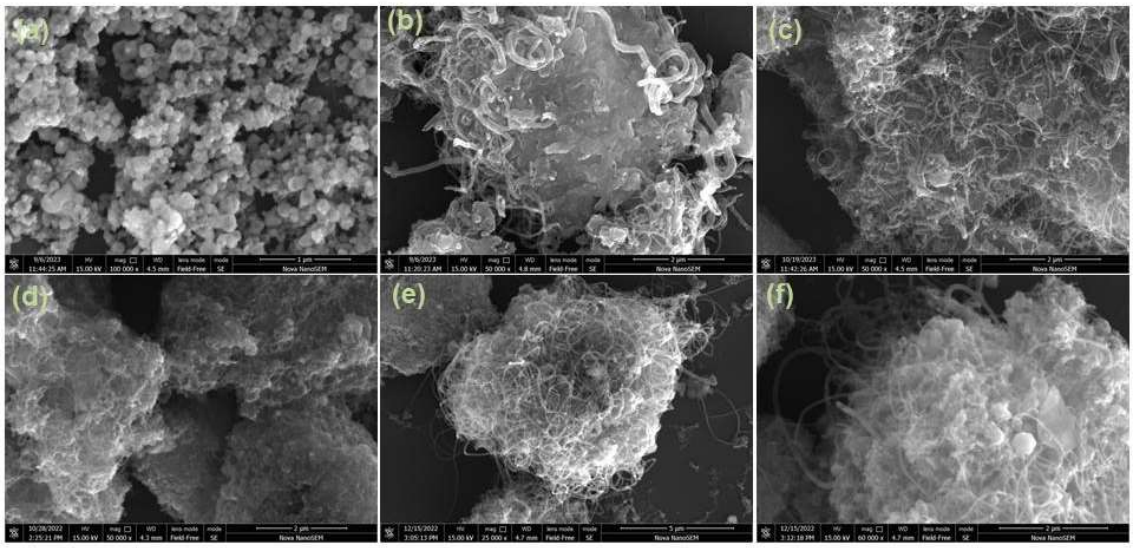

Figure S12. SEM images of (a) $CoFe_2O_4$, (b) CF10-N/C4-AW, (c) CF25-N/C1, (d) CF25-N/C2, (e) CF25-N/C3 and (f) CF25-N/C4.

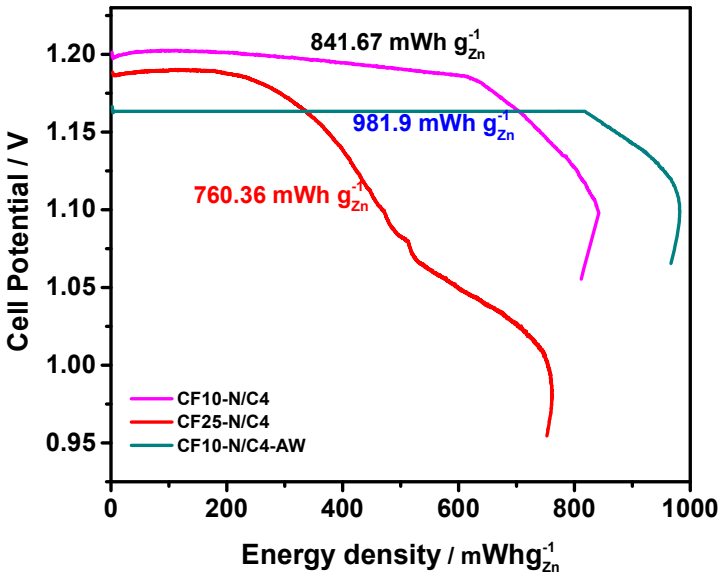

Figure S13. The gravimetric energy density with cell potential at various catalytic materials

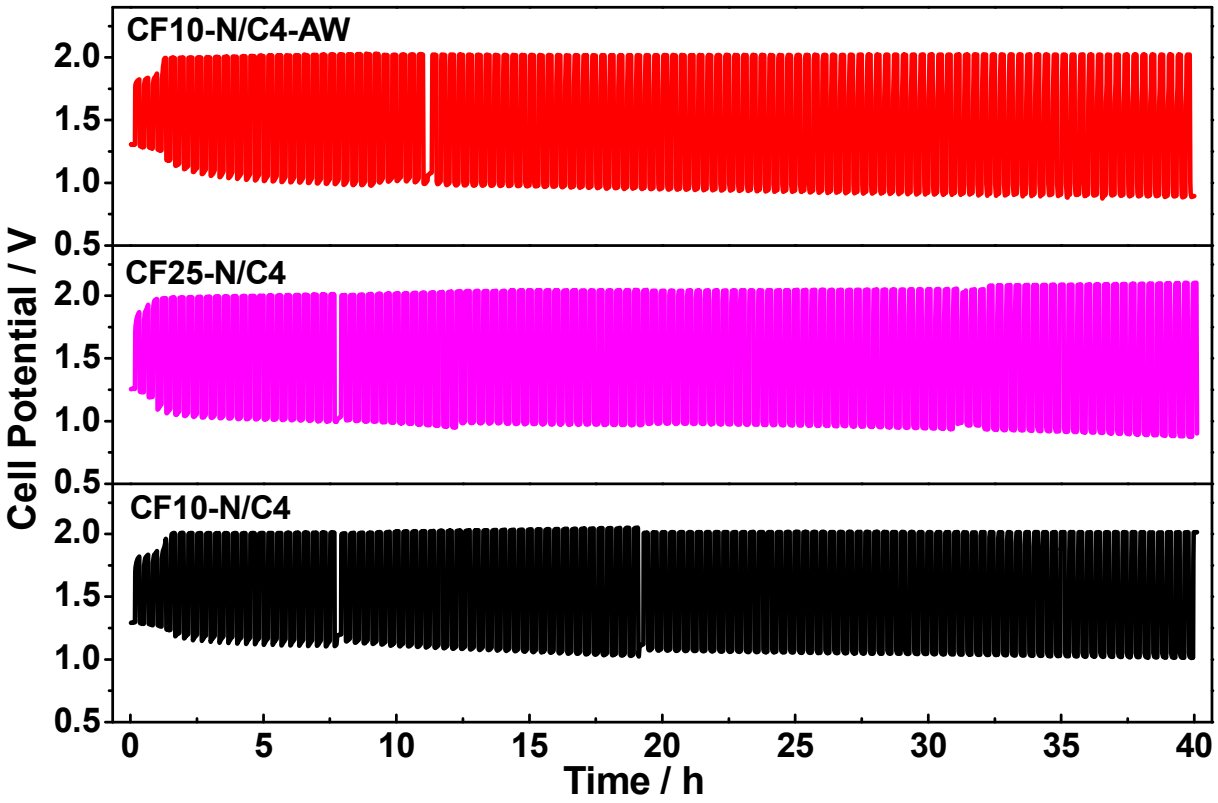

Figure S14. Galvanostatic charge-discharge cycling stability of CF10-N/C4, CF25-N/C4 and CF10-N/C4-AW composites at 5 mA cm^{-2} current density and 20 minutes per cycle in aqueous ZAB.

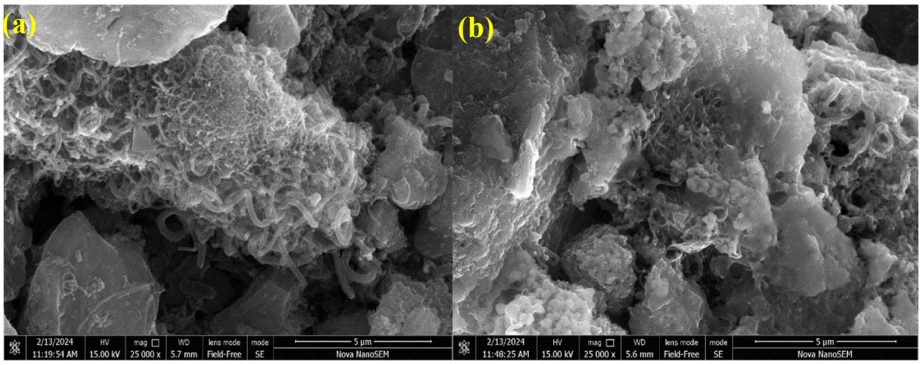

Figure S15. SEM images of the CF10-N/C4 on the carbon paper (a) before and (b) after the zinc-air battery testing.

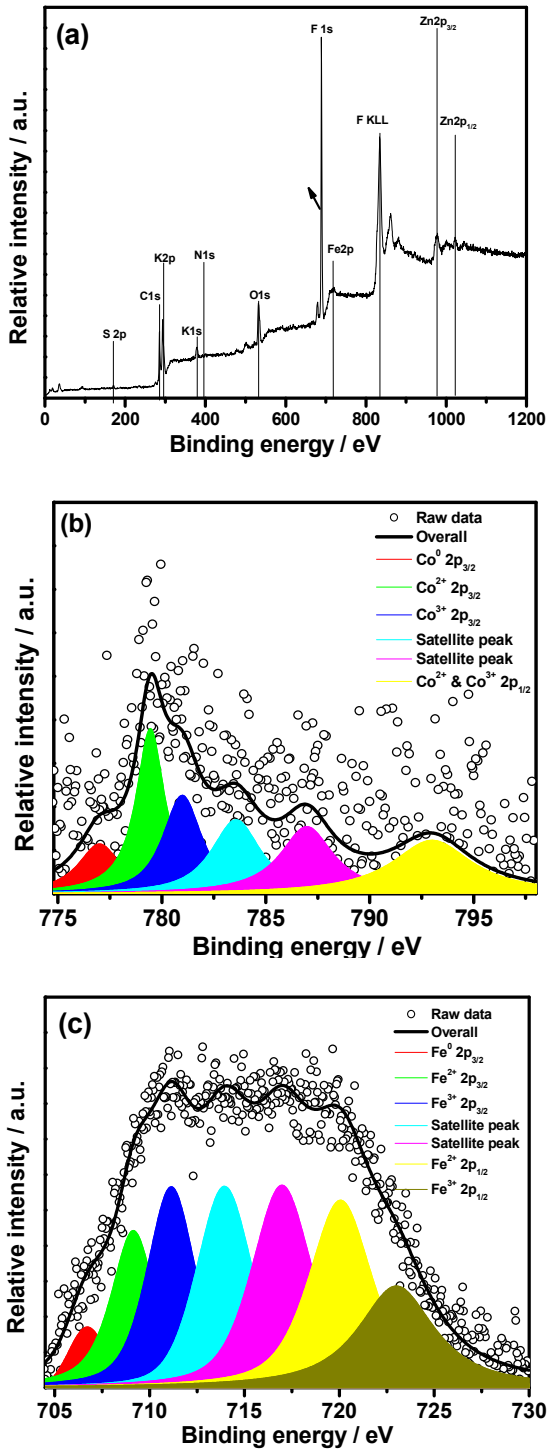

Figure S16. (a) Survey spectrum of the CF10-N/C4 coated on carbon paper after the zinc-air battery testing. Deconvoluted spectra of (b) Co-2p and (c) Fe-2p peaks after battery testing.

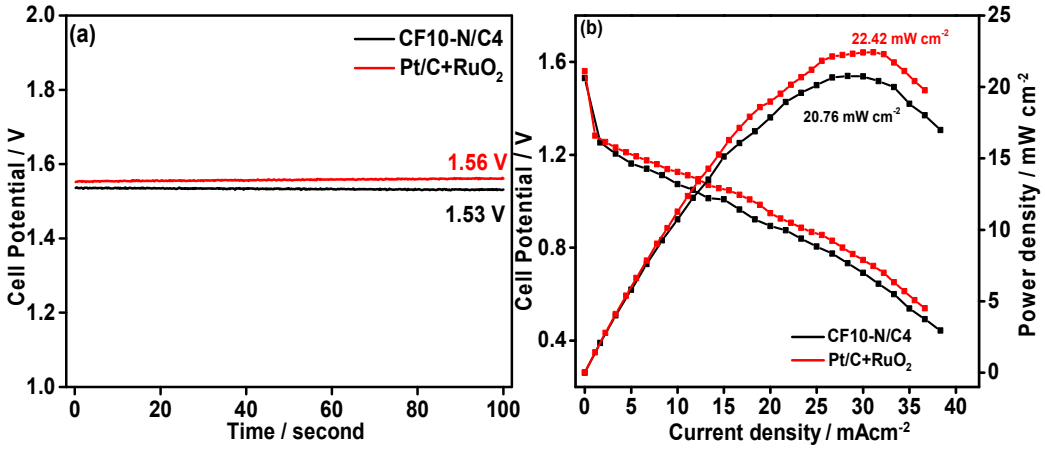

Figure S17. (a) Open circuit potential and (b) polarisation plot of CF10-N/C4 and Pt/C+RuO_2 in solid-state Zn-air battery

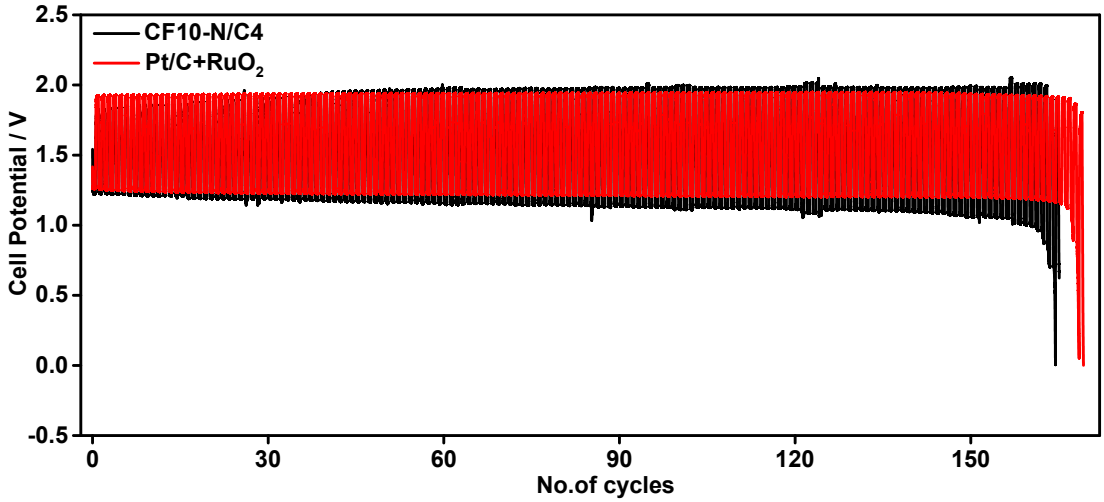

Figure S18. Galvanostatic charge-discharge cycling stability of CF10-N/C4 composite at 1 mA cm^{-2} current density and 2 minutes per cycle compared with Pt/C+RuO_2 in solid-state ZAB.

Table S1. The percentage of the elements present in the catalytic materials using EDAX

Material	C	N	O	Co	Fe
CF10-N/C4	85.8	9.7	3.2	0.5	0.8
CF25-N/C4	76.3	13.8	7.8	0.8	1.3

Table S2. Electrical conductivity of the catalysts measured from the I-V measurements (2 probe method)

Materials	Conductivity (S m^{-1})
$CoFe_2O_4$	7.8×10^{-7}
CF10-N/C4	1.6
CF25-N/C4	0.5

Table S3. The literature reported ORR activity in the alkaline medium of $CoFe_2O_4$-based materials.

S. No	Material	E_0 / V	$E_{1/2}$ / V	n	Reference
1.	Vo-CoFe/$CoFe_2O_4$@NC	-	0.86	3.9	1
2.	$CoFe_2O_4$-VC	-	0.69	3.7	2
3.	$CoFe_2O_4$-NC	0.98	0.86	3.8	3
4.	$CoFe_2O_4$-Biocarbon	0.82	-	3.9	4
5.	CoFe-N-GCNT	1.06	0.88	3.6	5
6.	CoFe-NC	-	0.88	3.9	6
7.	$FeZn_4Co$@CNF	-	0.84	3.8	7
8.	$CoFe_2O_4$-NCNT/FA	0.93	0.81	3.96	8
9.	FeOx@CoOx/NC2	1.03	0.89	3.8	9
10.	CoFe–CoCX@NCNT	1.01	0.89	3.9	10
11.	CoFe@C NBs	1.02	0.90	3.9	11
12.	CoFe-NC	0.99	0.87	3.96	12
13.	CoFe/Se@CN	-	0.87	3.98	17
14.	CoFe-$CoFe_2O_4$@NC	-	0.83	3.98	18
15.	CoFe@NC/CoFe2O4/IF	0.93	0.85	3.75	19
16.	CoFe@NCT	0.99	0.84	3.93	20
17.	CF10-N/C4	1.00	0.84	3.8	This work
18.	CF25-N/C4	0.95	0.81	3.8	This work
19.	CF10-N/C4-AW	0.95	0.80	3.5	This work

Table S4. Comparison of the Zn-air battery activities of $CoFe_2O_4$-based materials.

S. No.	Material	OCP (V)	Power density (mW cm^{-2})	Specific capacity (mA h g_{Zn}^{-1})	Reference
1.	Vo-CoFe/CoFe2O4@NC	1.53	138.5	774.8	1
2.	CoFe-N-GCNT	1.49	133	-	5
3.	FeZn4Co@CNF	1.49	107.6	796.8	7
4.	CoFe–CoCX@NCNT	1.42	175	-	10
5.	CoFe-NC	1.47	132	703	12
6.	CoFe-NC@CC	1.47	154.2	-	13
7.	CoFe@NCNT	1.45	150	808	14
8.	CoN/Cnet@Co2Fe@NCNT	1.47	235.5	-	15
9.	CoFe/Se@CN	1.48	160	802	17
10.	CoFe-$CoFe_2O_4$@NC	1.51	106.32	785	18
11.	CoFe@NC/CoFe2O4/IF	1.48	134.5	-	19
12.	CoFe@NCT	1.49	194	795	20
13.	CF10-N/C4	1.53	159	767.06	This work
14.	CF25-N/C4	1.50	134.7	785.25	This work
15.	CF10-N/C4-AW	1.50	162	900	This work

References

1. Y. Go, K. Min, H. An, K. Kim, S. Eun Shim and S.-H. Baeck, *Chem Eng J*, 2022, 448, 137665.
2. S. Zhao, T. Guo, J. Fan, L. Wang, M. Han, J. Wang, Y. Wu, and Y. Chen. *Energy Fuels,* 2020, 34, 9069−9075.
3. H. Wang, C. Liu, X. Yang, J. Gu, M. Niu, L. Yang, Z. Bai. *Int J Hydrogen Energ.,* 2022, 47, 6059-6066.
4. S. Liu, W. Bian, Z. Yang, J. Tian, C. Jin, M. Shen, Z. Zhou and R. Yang. *J. Mater. Chem. A*, 2014,2, 18012 –18017.
5. L. Liu, D. Hui Wu, L. Zhang, J. Feng, A. Wang. *J. Colloid Interface Sci.,* 2023, 639, 424–433.
6. J. Ma, Q. Wu, W. Zhang, Y. Li, Y. Lu, B. Liu, F. Yang, Y. Song. *Electrochim. Acta*, 2022, 432, 141224.
7. F. Wang, Z. Xiao, X. Liu, J. Ren, T. Xing, Z. Li, X. Li, Y. Chen. *J. Power Sources*, 2022, 521, 230925.
8. Q. Huang, C. Li, Y. Tu, Y. Jiang, P. Mei, X. Yan. *Ceram. Int.,* 2021, 47, 1602-1608.
9. F. Nasim, H. Ali, M. Nadeem and M. Nadeem. *Sustain. Energy Fuels,* 7, 2023, 190.
10. J. Sun, N. Guo, T. Song, Y. Hao, J. Sun, H. Xue, Q. Wang. *Adv. Powder Mater.,* 2022, 1, 100023.
11. L. Liu, Z. Xu, T. Lu, Z. Wang, X. Shi, C. Li, Y. Wei, Z. Zi. *J Alloy Compd.*, 2022, 906, 164296.
12. W. Li, M. Zhang, X. Xie, A. Liang, H. Peng, G. Ma, and Y. Xu. https://doi.org/10.1021/acsanm.3c03751.
13. Q. Liu, X. Liu, Y. Xie, F. Sun, Z. Liang, L. Wang and H. Fu. *J. Mater. Chem. A,* 2020, 8, 21189.
14. P. Cai, Y. Hong, S. Ci and Z. Wen. *Nanoscale*, 2016, 8, 20048.
15. T. Qin, J. Niu, X. Liu, C. Geng, and A.P. O'Mullane. *ACS Appl. Mater. Interfaces* 2023, 15, 7987−7998.
16. A.M. Abdallah and R. Awad. *Physica B Condens. Matter,* 2021, 608, 412898.
17. L. Dai, C. Feng, Y. Luo, J. Wan, Y. Sun, Y. Zheng, H. Zhang, and Y. Wang. *Chem. Eur. J.,* 2024, 30, e202303173.
18. J. Zou, T. Liang, M. Peng, P. Liu, Z. Li, J. Wen, Z. Li, Y. Yan, X. Yu, X. Zeng, J. Huang. *J. Energy Storage,* 2024, 84, 110815.

19. J. Lai, C. Zeng, S. Peng, Q. Zhou, J. Zeng, C. Liu, X. Qi. *J. Power Sources,* 2024, 599, 234218.
20. M. Wang, B. Liu, H. Zhang, Z. Lu, J. Xie, Y. Cao. *J. Colloid Interface Sci.,* 2024, 661, 681–689.